〈Research Article〉

Label-free and Sensitive Detection of Purine Catabolites in Complex Solutions by Surface-enhanced Raman Spectroscopy

Batmend Davaa-Ochir[a,b], Iris Baffour Ansah[a,b], Sung Gyu Park[a], Dong-Ho Kim[a,b*]

[a]Nano-Bio Convergence Department, Korea Institute of Materials Science (KIMS), Changwon, Gyeongnam 51508, Republic of Korea
[b]Advanced Materials Engineering Division, University of Science and Technology (UST), 217 Gageong-ro, Yuseong-gu, Daejeon 34113, Republic of Korea

Abstract

Purine catabolite screening enables reliable diagnosis of certain diseases. In this regard, the development of a facile detection strategy with high sensitivity and selectivity is demanded for point-of-care applications. In this work, the simultaneous detection of uric acid (UA), xanthine (XA), and hypoxanthine (HX) was carried out as model purine catabolites by surface-enhanced Raman Spectroscopy (SERS). The detection assay was conducted by employing high-aspect ratio Au nanopillar substrates coupled with in-situ Au electrodeposition on the substrates. The additional modification of the Au nanopillar substrates via electrodeposition was found to be an effective method to encapsulate molecules in solution into nanogaps of growing Au films that increase metal-molecule contact and improve substrate's sensitivity and selectivity. In complex solutions, the approach facilitated ternary identification of UA, XA, and HX down to concentration limits of 4.33 μM, 0.71 μM, and 0.22 μM, respectively, which are comparable to their existing levels in normal human physiology. These results demonstrate that the proposed platform is reliable for practical point-of-care analysis of biofluids where solution matrix effects greatly reduce selectivity and sensitivity for rapid on-site disease diagnosis.

Keywords : Surface-enhanced Raman spectroscopy; Au nanopillars; electrodeposition; hotspots; uric acid; xanthine; hypoxanthine.

1. Introduction

Surface-enhanced Raman spectroscopy (SERS) is a useful analytical tool for biological and chemical characterizations. The technique is utilized in various sensing platforms for molecular identification and quantification due to its prominent ability to amplify Raman fingerprint signals of molecules adsorbed on noble metals [1-8]. Typically, the enhancement effect of SERS is dependent on electromagnetic enhancement (EM) and chemical enhancement (CE) factors that stem from localized surface plasmon resonance (LSPR) generated in near-field of metals and charge transfer processes, respectively [9]. The EM effect is dominant in maximizing SERS activity in most analytical settings. Hence, plasmonic nanostructures are salient to achieve strong electric field localization ("hotspots") at metal nanogaps that intensify Raman signals of adsorbates (up to $\approx 10^8$), allowing single-molecule detections [10]. Despite of this merit, the existence of multiple Raman-active species in complex samples presents a limitation in expanding SERS techniques to real systems since the competitive adsorption and the surface

*Corresponding Author: Dong-Ho Kim
Nano-Bio Convergence Department, Korea Institute of Materials Science
Tel: +82-55-280-3557; E-mail: dhkim2@kims.re.kr

fouling reduce selectivity and sensitivity for reliable on-site applications [11-15]. There is a growing interest to explore and develop facile methods to boost specificities in metal-molecule contact on SERS substrates for practical advancement.

A strategy to address the aforementioned limitation can be proposed through electrokinetic actuations where the application of electric fields to SERS substrates facilitates electrostatic interactions for selective adsorption of molecules at metal nanogaps [16, 17]. For example, Etchegoin et al. [18] demonstrated the influence of electrostatics in guiding charged species (Nile blue) towards Ag colloids for signal enhancement, while Jeong et al. [19] employed the technique to sense serotonin on Ag nanoislands through molecule confinement in volumetric hotspots by electrokinetic preconcentration. Despite these remarkable efforts, the challenge of ultrasensitivity and selectivity for analysis involving complex solutions still remains since target molecules are exposed to limited density of pre-formed nanogaps (or hotspots) and several interfering species adversely affect target adsorption [11, 12, 20]. In this regard, the present study utilizes an electrochemical-SERS (EC-SERS) strategy that greatly improves sensitivity and selectivity for complex solutions through in-situ growth of metal layers on SERS electrodes by electrodeposition and simultaneous electrokinetic attraction of molecules into interstitial voids of the substrates for improving metal-molecule contact within plasmonic nanogaps.

2. Experimental Section

2.1. Materials

Uric acid ($C_5H_4N_4O_3$), xanthine ($C_5H_4N_4O_2$), hypoxanthine ($C_5H_4N_4O$), sodium hydroxide (NaOH), gold (III) chloride trihydrate ($HAuCl_4 \cdot 3H_2O$) were purchased from Sigma-Aldrich (St. Louis, MO, USA). Sodium chloride (NaCl) was purchased from Samchun (Pyeongtaek, South Korea).

2.2. Fabrication of Au nanopillar electrodes as SERS substrates

Au nanopillar electrodes were fabricated using polyethylene terephthalate (PET) as the underlying substrate. Nanopillar structures were generated on the PET by treating the substrate with CF_4 plasma (100 W, 3 sccm, 56 mTorr) for 2 min with a 13.56 MHz radio-frequency ion etching apparatus [12]. The CF_4 plasma was employed to control the topology wettability of the surface by forming the fluorinated carbon layer [29]. Afterwards, the substrate was treated with Ar plasma for 1 min (100 W). Au was deposited onto the generated nanopillars to a thickness of 200 nm using a sputtering system. The fabricated substrates were characterized by field-emission scanning electron microscopy (FE-SEM; Jeol JSM-6700F).

2.3. Electrochemical–SERS instrumentation and measurements

An Ocean Optics probe spectrometer (UQEPRO-Raman) was used for SERS measurements and electrochemical Au deposition was conducted with a portable ZIVE SP_2 Wonatech potentiostat [30, 31]. An electrodeposition chamber that holds the Au nanopillar electrode, Ag/AgCl (in 3 M NaCl) reference electrode, platinum counter electrode, and solution analyte was employed. The electrodeposition cell was filled with 0.1 M NaCl aqueous solution (378 µL) as the supporting electrolyte. Ten microliters of target analyte solutions in desired concentrations were added to the NaCl electrolyte. Then, 12 µL of 100 mM $HAuCl_4$ (dissolved in DIW) was added into the cell and the analyte was carefully mixed. The final concentration of $HAuCl_4$ in the solution was 3 mM. The analyte was exposed to the laser and a constant electric potential (+0.1

V vs Ag/AgCl) was applied to the electrode for Au electrodeposition. During the entire deposition period, SERS data were recorded in real-time at an integration time of 10 s. The laser power for measurements was 40 mW. All electrode potentials are reported vs Ag/AgCl reference electrode.

3. Results and discussion

3.1. SERS detection of UA, XA, and HX by on bare Au nanopillar electrode

Au nanopillar electrodes were employed as SERS-active substrates in this study. The intrinsic performance of the as-prepared electrodes was investigated by measuring SERS signals of UA, XA, and HX aqueous solutions. Figure 1a shows that rich fingerprint signals with significant intensities is obtainable for all target molecules at high concentration level (i.e., 200 µM) enabling their direct identification. Thus, characteristic SERS peaks of UA were observed at 494, 590, 639, 782, 816, 896, 964, 1076, 1132, 1209, 1374, 1569, and 1650 cm^{-1}. Those of XA were 508, 572, 653, 869, 958, 1126, 1243, 1312, 1368, 1476, 1555, and 1699 cm^{-1}. HX peaks were obtained at 544, 597, 632, 725, 964, 1019, 1085, 1300, 1333, 1365, 1412, 1470, 1535, 1598, and 1716 cm^{-1}

(vibrational assignments corresponding to SERS peaks is summarized in Table 1 [12, 32-36]). Lower concentrations of the targets were then analyzed to ascertain the electrodes' sensitivity. For measurements involving 10 µM analyte solutions, SERS signal of UA was indistinguishable from the background signal of the bare electrode and low intensities of XA and HA were recorded (Fig. 1b) which can be ascribed to weak contact between the metal and molecules which are randomly distributed in solution. In order to improve the plasmonic activity of the electrodes for superior detection sensitivity, the Au nanopillars were modified via Au electrodeposition.

3.2. SERS signal amplification of UA, XA, and HX by Au electrodeposition

The electrode modifications were performed in the presence of target molecules for maximized sensing performance by in-situ encapsulating the molecules within growing Au structures that ensures close metal-molecule proximity at the nanogaps of nanopillar structures [2, 11, 31, 37, 38]. For this purpose, target analytes were dissolved in HAuCl$_4$ aqueous solution and injected into a custom-built electrodeposition chamber that embedded Au nanopillar electrodes. An
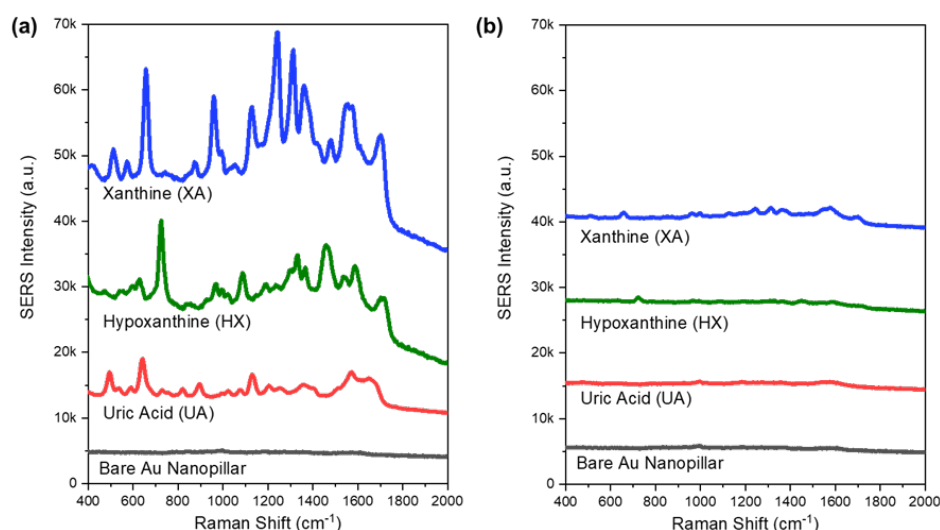

Fig. 1. SERS signals of (a) 200 µM and (b) 10 µM uric acid, xanthine, hypoxanthine aqueous solutions measured on bare Au nanopillar electrodes.

Table 1. Peak assignments for UA, XA, and HX SERS signals measured on Au nanopillars electrode.

Uric Acid		Xanthine		Hypoxanthine	
Peak Position (cm^{-1})	Assignment	Peak Position (cm^{-1})	Assignment	Peak Position (cm^{-1})	Assignment
494	C–N–C ring vibration	508	Ring torsion	544	Ring deformation (enolic)
590	Ring breathing	572	Ring breathing	597	Ring breathing
639	Skeletal ring deformation	653	Ring plane bending	632	Ring breathing
782	Ring vibration	869	C–N plane bending	725	Purine ring breathing
816	Ring vibration	958	N–C stretching	964	N–C–N ring bending
896	N–H bending	1126	N–C stretching, N–H bending	1019	C–H bending
964	Ring vibration	1243	C–H bending	1085	C–N, N–H rocking
1076	Ring vibrations, C–O, C–C, C–N, N–C–C stretching and bending	1312	Ring stretching	1300	C–H rocking
1132	Ring stretching and bending	1368	N–H bending, C–H bending	1333	C–H rocking, ring breathing
1209	N–C–C stretching and bending	1476	H–C–N bending	1365	C–H, N–H rocking, C-N stretching
1374	C–O stretching	1555	C=C stretching, N–H bending, C–H bending	1412	N–H, C–H, N–H rocking, imidazole ring deformation
1569	C–N stretching	1699	C=O stretching, N–H bending	1470	C–H rocking
1650	C=O stretching			1535	Imidazole ring stretching
				1597	C–=N stretching
				1718	C=O stretching

electric potential (i.e., +0.1 V vs Ag/AgCl) relatively lower than the reduction potential of HAuCl$_4$ (i.e., 0.79 V vs Ag/AgCl [30]) was then ap plied to the electrodes to convert Au^{3+} to metallic Au [11, 12, 31]. Here, the influence of growing new Au nanostructures was assessed by comparing SERS signals measured during external potential application in the absence and presence of HAuCl$_4$. As depicted in Figure 2a, signal intensities of UA, XA, and HX (10 µM each) were amplified 14, 17, and 23 folds, respectively, with Au electrodeposition. The spectral evolution plots in Figure 2b − 2d further substantiate the dynamic enhancement of weak UA, XA, and HA signals at the onset of deposition, from which signal intensities rapidly amplified and attained maximum enhancement between 70 s and 100 s.
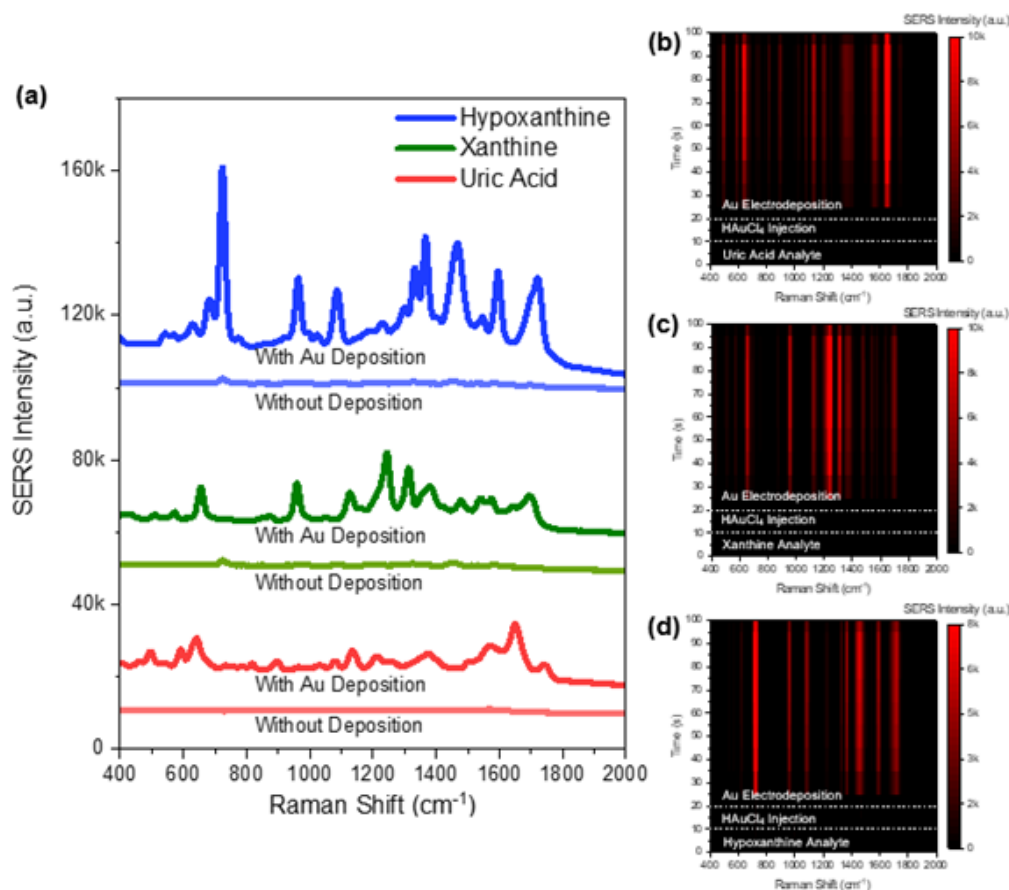

Fig. 2. (a) SERS signals measured with and without Au electrodeposition for 10 µM UA (red lines), 10 µM XA (green lines), and 10 µM HX (blue lines) on Au nanopillar electrodes. Dynamics of SERS signal evolution of (b) uric acid, (c) xanthine, and (d) hypoxanthine before and during Au electrodeposition.

dynamic enhancement of weak UA, XA, and HA signals at the onset of deposition, from which signal intensities rapidly amplified and attained maximum enhancement between 70 s and 100 s.

The rapid and strong enhancement of SERS signals is ascribed to a complementary effect of the electric potential that reduces HAuCl4 to new Au structures and simultaneously attract charged molecules to hotspot zone of the nanopillars. To elucidate the former, the surface morphologies of the electrodes before and after the Au electrodeposition were compared as shown in Figure 3. Even though the effect of target analyte on the Au deposition (Figure 3b – 3d) is not noticeable, the size of nanopillars after the deposition was increased about 1.3 times compared to the pristine one (Figure 3a). The resultant narrowed inter-pillar gaps can provide improved EM enhancement for SERS signal amplification.

The entrapment of target molecules during in-situ deposition can be ascribed to the significant signal amplification. In order to investigate the target entrapment, the SERS measurements were carried out for the post addition of target molecules after Au electrodeposition. Surprisingly, the SERS signal intensity is quite low in the post addition cases (Figure 4). It confirms that the approach of modifying Au nanopillars through in-situ Au electrodeposition is advantageous for rapid and ultra-high sensitive detection of the catabolites.

3.3. Ternary detection of UA, XA, and HX in complex solution by Au electrodeposition

The feasibility of the method for complex sample analysis was investigated through ternary detection of UA, XA, and HX. SERS analysis of the mixture solution was first performed on bare Au nanopillars to ascertain the selectivity of the electrode. In Figure 5a (black spectrum), only weak SERS peaks (725 and 1470 cm^{-1}) characteristic to hypoxanthine were identifiable in the UA:XA:HX mixture attributed to competitive adsorption at the limited hotspot regions of the nanopillar electrode [39]. To improve both sensitivity and selectivity for the complex mixture analysis, Au electrodeposition was performed according to the previously described protocol.

Fig. 4. SERS signals measurements carried out by in situ Au electrodeposition (at +0.1 V) in the presence of target molecules and those carried out by introducing target after the Au electrodeposition for 10 μM UA (red lines), 10 μM XA (green lines), and 10 μM HX (blue lines) on Au nanopillar electrodes.
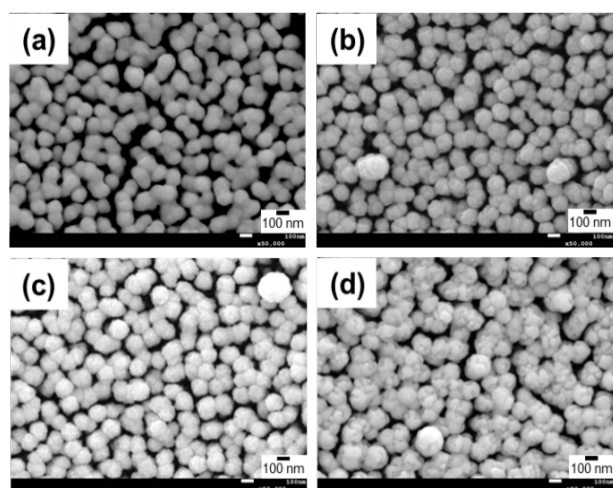

Fig. 3. Scanning electron microscopy (SEM) images of (a) as-prepared nanopillar electrode after Au electrodeposition in the presence for (b) uric acid, (c) xanthine, (d) hypoxanthine.
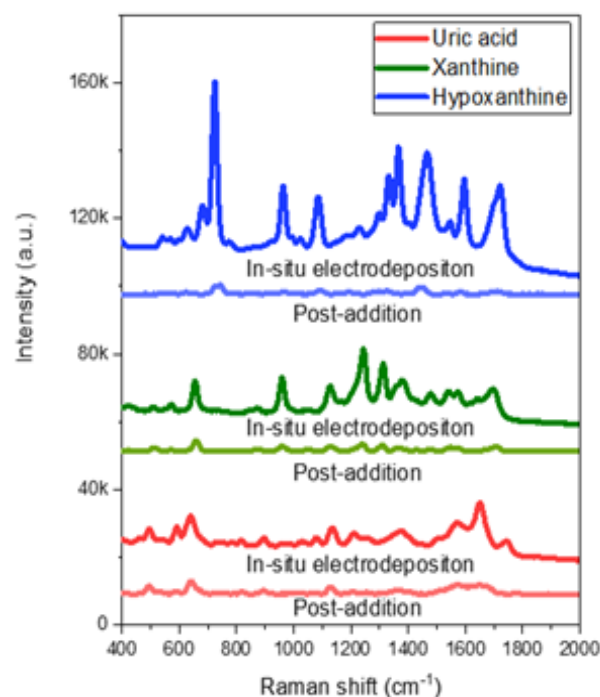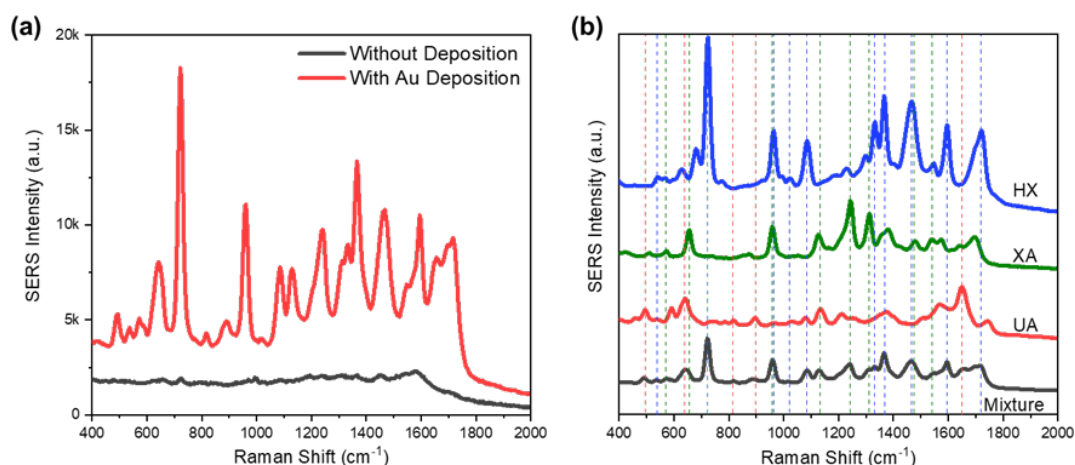
Fig. 5. (a) SERS measurement on Au nanopillar substrate for UA:XA:HX ternary mixture with and without Au electrodeposition and (b) SERS peak assignment of uric acid, xanthine, and hypoxanthine in the ternary mixture. The red, blue and green dashed lines correspond to the uric acid, xanthine, and hypoxanthine peaks, respectively, that appear in the UA:XA:HX mixture SERS spectrum.

From Figure 5a (red spectrum), SERS signal of the UA:XA:HX mixture was improved by 28-folds with Au electrodeposition. Importantly, the influence of the deposition was strongly accomplished in the selective enhancement of fingerprint peaks of all targets in the complex mixture for direct identification. As illustrated in Figure 5b, SERS signals at 494, 816, 896, and 1560 cm^{-1} originate from UA. XA exhibited peaks at 572, 1126, 1243, 1312, and 1538 cm^{-1} while HX was identified by peaks at 544, 725, 1019, 1085, 1333, 1365, 1598, and 1718 cm^{-1}. Meanwhile, peaks at 642 cm^{-1} was assigned as a contribution from both UA and XA and those at 958 and 1467 cm^{-1} originate from both XA and HX. It is evident that the sensitive and selective identification of multiple analytes can be accomplished with this approach.

3.4. Au electrodeposition optimization

To assess the ideal sensing performance for complex solution analysis, the parameters for Au deposition was optimized by varying the electric potential and HAuCl$_4$ concentration. The optimization is based on the concurrent consideration of the characteristic peak intensities of the three target molecules (721 cm^{-1} for HX, 1243 cm^{-1} for XA, and 1647 cm^{-1} for UA). First, a potential range of +0.7 V to −0.1 V was investigated in the presence of 3 mM HAuCl$_4$. In Figure 6a, the SERS signal of UA:XA:HX was lowest when −0.1 V and +0.7 V potentials were applied. Higher signal intensities were obtained for +0.1 V, +0.3 V
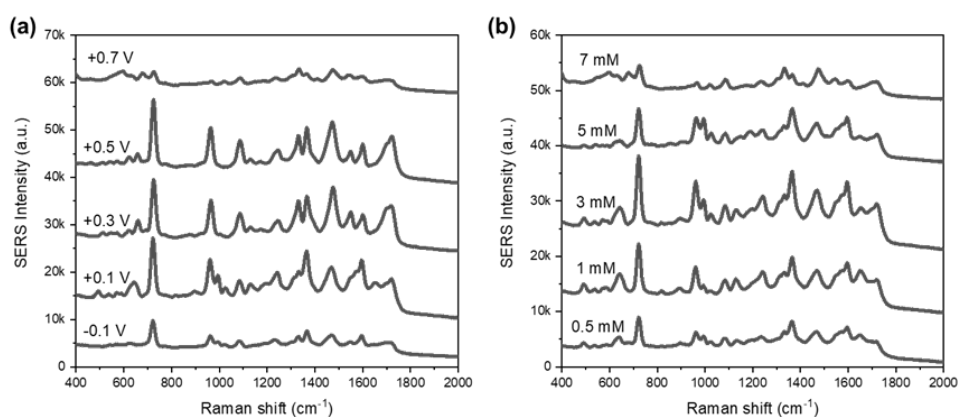

Fig. 6. SERS spectra for a UA:XA:HX ternary mixture at (a) varied electrodeposition potentials and (b) HAuCl$_4$ concentrations.

and +0.5 V. Even though there is no significant difference from +0.1 V to +0.5 V, the potential of +0.1 V was chosen as the optimum value since the superior signal selectivity can be obtained especially for weak UA characteristic signal. Subsequently, +0.1 V was maintained as $HAuCl_4$ concentration varied from 0.5 mM to 7 mM. As depicted in Figure 6b, the system with 3 mM $HAuCl_4$ demonstrated superior sensitivity for Raman signals of all components in the complex mixture solution.

3.5. Detection sensitivity analysis and quantification of UA, XA, and HA in complex solutions

The sensitivity of this method was evaluated by analyzing ternary mixtures of various concentrations of UA:XA:HX. Here, XA and HX concentrations were set to be 10-times lower than UA considering the physiological levels at which they exist in biological fluids.

For instance, in human aqueous humor, UA, XA, and HX concentrations are in the range of 41.10 − 50.14 μM, 2.43 − 3.22 μM, and 0.4 − 1.8 μM, respectively [22, 25]. Under the optimized Au deposition conditions, signal intensity of UA:XA:HX solutions changed proportionally to concentration from 200 μM to 5 μM for UA, and 20 μM to 0.5 μM for both XA and HX (Figure 7a). SERS peaks at 1647, 1243, and 721 cm^{-1} were designated as UA, XA, and HX peaks for quantification; the limit of detections (LOD) and regression for each target was evaluated in the presence of the other two targets. The LODs for UA, XA, and HX in the ternary mixture were determined as 4.33 μM, 0.71 μM, and 0.2 μM, respectively. Along the entire concentration ranges investigated, peak intensity-to-concentration correlations for all targets exhibited Langmuir isotherm models (Figure 7b-d) according to the regression equation:
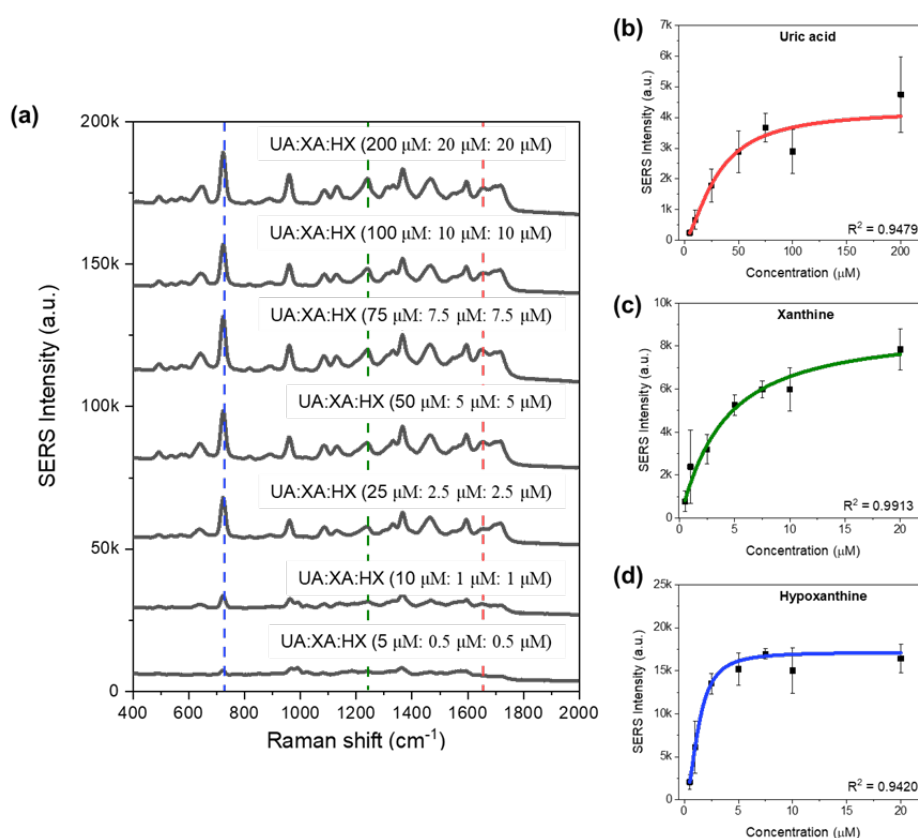

Fig. 7. (a) SERS signals of UA:XA:HX ternary mixtures with various component concentrations. The red, green, and blue dashed lines are characteristic peaks assigned for calibration for uric acid, xanthine, and hypoxanthine, respectively. Linear correlations between signal intensities and the concentrations for (b) uric acid, (c) xanthine, and (d) hypoxanthine.

$$I = \frac{\alpha K_L C}{1 + K_L C} \qquad (1)$$

where I corresponds to the signal intensity, α represents Langmuir isotherm constant, K_L is adsorption constant and C is molar concentration [12]. The regression coefficients (R^2) were estimated as 0.9479, 0.9913, and 0.9420, for UA, XA, and HX, respectively, indicating the good reliability of the method for practical applications.

4. Conclusion

In summary, this work demonstrates a facile electrochemical-SERS method for ternary label-free detection of uric acid (UA), xanthine (XA), and hypoxanthine (HX) on Au nanopillar electrodes. Owing to the challenge of selectivity and sensitivity for complex mixture analysis on bare Au electrodes, the Au nanopillars were modified via additional in-situ Au deposition to improve the electrodes' plasmonic properties and ensure close metal-molecule contact in nanogap spaces for selective Raman signal enhancement. Resultantly, simultaneous sensitive detection and quantification of UA, XA, and HX was realized by label-free SERS methods. It is promising that the detection limits (4.33 μM, 0.71 μM, and 0.2 μM for UA, XA, and HX, respectively) are comparable to the physiological levels in normal human. We believe this study can broaden the versatility of SERS platforms for reliable point-of-care diagnostic applications. In near future, this protocol is going to be used for analysis of aqueous humor samples for diagnosing eye diseases such as retinoblastoma and age-related macular degeneration.

References

[1] D. Cialla, A. März, R. Böhme, F. Theil, K. Weber, M. Schmitt, J. Popp, Surface-enhanced raman spectroscopy (SERS): progress and trends, Anal. Bioanal. Chem., 403(2012) 27-54.

[2] S. Kim, I. B. Ansah, J. S. Park, H. Dang, N. Choi, W. C. Lee, S. H. Lee, H. S. Jung, D. H. Kim, S. M. Yoo, J. Choo, S. H. Kim, S. G. Park, Early and direct detection of bacterial signaling molecules through one-pot Au electrodeposition onto paper-based 3D SERS substrates, Sens. Actuators B Chem., 358(2022) 131504.

[3] E. H. Koh, W. C. Lee, Y. J. Choi, J. I. Moon, J. Jang, S. G. Park, J. Choo, D. H. Kim, H. S. Jung, A wearable surface-enhanced raman scattering sensor for label-free molecular detection, ACS Appl. Mater. Interfaces, 13(2021) 3024-3032.

[4] C. Li , Y. Huang, X. Li, Y. Zhang, Q. Chen, Z. Ye, Z. Alqarni, S. E. J. Bell, Y. Xu, Towards practical and sustainable SERS: a review of recent developments in the construction of multifunctional enhancing substrates, J. Mater. Chem. C, 9(2021) 11517-11552.

[5] V. T. N. Linh, J. Moon, C. W. Mun, V. Devaraj, J. W. Oh, S. G. Park, D. H. Kim, J. Choo, Y. I. Lee, H. S. Jung, A facile low-cost paper-based SERS substrate for label-free molecular detection, Sens. Actuators B Chem., 291(2019) 369-377.

[6] V. T. N. Linh, S. G. Yim, C. W. Mun, J. Y. Yang, S. Lee, Y. W. Yoo, D. K. Sung, Y. I. Lee, D. H. Kim, S. G. Park, S. Y. Yang, H. S. Jung, Bioinspired plasmonic nanoflower-decorated microneedle for label-free intradermal sensing, Appl. Surf. Sci., 551(2021) 149411.

[7] B. Sharma, R. R.Frontiera, A. I. Henry, E. Ringe, R. P.V. Duyne, SERS: Materials, applications, and the future, Mater. Today, 15(2012) 16-25.

[8] C. W. Mun, V. T. N. Linh, J. D. Kwon, H. S. Jung, D. H. Kim, S. G. Park, Highly sensitiveand selective nanogap-enhanced SERS sensing platform, Nanomater., 9(2019) 619.

[8] C. W. Mun, V. T. N. Linh, J. D. Kwon, H. S. Jung, D. H. Kim, S. G. Park, Highly sensitive and selective nanogap-enhanced SERS sensing platform, Nanomater., 9(2019) 619.

[9] J. Langer, D. J. de Aberasturi, J. Aizpurua, R. A. A. Puebla, B. Auguié, J. J. Baumberg, G. C. Bazan, S. E. J. Bell, A. Boisen, A. G. Brolo, J. Choo, D. C. May, V. Deckert, L. Fabris, K. Faulds, F. J. G. de Abajo, R. Goodacre, D. Graham, A. J. Haes, C. L. Haynes, C. Huck, T. Itoh, M. Käll, J. Kneipp, N. A. Kotov, H. Kuang, E. C. Le Ru, H. K. Lee, J. F. Li, X. Y. Ling, S. A. Maier, T. Mayerhöfer, M. Moskovits, K. Murakoshi, J. M. Nam, S. Nie, Y. Ozaki, I. P. Santos, J. P. Juste, J. Popp, A. Pucci, S. Reich, B. Ren, G. C. Schatz, T. Shegai, S. Schlücker, L. L. Tay, K. G. Thomas, Z. Q. Tian, R. P. V. Duyne, T. V. Dinh, Y. Wang, K. A. Willets, C. Xu, H. Xu, Y. Xu, Y. S. Yamamoto, B. Zhao, L. M. L. Marzán, Present and future of surface-enhanced raman scattering, ACS Nano, 14(2020) 28-117.

[10] T. Y. Jeon, D. J. Kim, S. G. Park, S. H. Kim, D. H. Kim, Nanostructured plasmonic substrates for use as SERS sensors, Nano Converg., 2016. 3(2016) 18.

[11] I. B. Ansah, S. Kim, J. Y. Yang, C. W. Mun, H. S. Jung, S. Lee, D. H. Kim, S. H. Kim, S. G. Park, In situ electrodeposition of gold nanostructures in 3D ultra-thin hydrogel skins for direct molecular detection in complex mixtures with high sensitivity, Laser Photonics Rev., 15(2021) 2100316.

[12] I. B. Ansah, W. C. Lee, C. W. Mun, J. J. Rha, H. S. Jung, M. Kang, S. G. Park, D. H. Kim, In situ electrochemical surface modification of Au electrodes for simultaneous label-free SERS detection of ascorbic acid, dopamine and uric acid, Sens. Actuators B Chem., 353(2022) 131196.

[13] X. Xie, D. P. Wang, C. Guo, Y. Liu, Q. Rao, F. Lou, Q. Li, Y. Dong, Q. Li, H. B. Yang, F. X. Hu, Single-atom ruthenium biomimetic enzyme for simultaneous electrochemical detection of dopamine and uric acid, Anal. Chem., 93(2021) 4916-4923.

[14] W. Zhang, L. Liu, Y. Li, D. Wang, H. Ma, H. Ren, Y. Shi, Y. Han, B. C. Ye, Electrochemical sensing platform based on the biomass-derived microporous carbons for simultaneous determination of ascorbic acid, dopamine, and uric acid, Biosens. Bioelectron., 121(2018) 96-103.

[15] D. Ji, Z. Liu, L. Liu, S. S. Low, Y. Lu, X. Yu, L. Zhu, C. Li, Q. Liu, Smartphone-based integrated voltammetry system for simultaneous detection of ascorbic acid, dopamine, and uric acid with graphene and gold nanoparticles modified screen-printed electrodes, Biosens. Bioelectron., 119(2018) 55-62.

[16] R. Moldovan, E. Vereshchagina, K. Milenko, B. C. Iacob, A. E. Bodoki, A. Falamas, N. Tosa, C. M. Muntean, C. Farcău, E. Bodoki, Review on combining surface-enhanced Raman spectroscopy and electrochemistry for analytical applications, Anal. Chim. Acta, 1209(2022) 339250.

[17] D. Y. Wu, J. F. Li, B. Ren, Z. Q. Tian, Electrochemical surface-enhanced Raman spectroscopy of nanostructures, Chem. Soc. Rev., 37(2008) 1025-1041.

[18] P. D. Lacharmoise, E. C. L. Ru, P. G. Etchegoin, Guiding molecules with electrostatic forces in surface enhanced raman spectroscopy, ACS Nano, 3(2009) 66-72.

[19] M. Park, Y. J. Oh, S. G. Park, S. B. Yang, K. H. Jeong Electrokinetic preconcentration of small molecules within volumetric electromagnetic hotspots in surface enhanced raman scattering, Small, 11(2015) 2487-2492.

[20] M. L. B. Figueiredo, C. S. Martin, L. N Furini, R. J. G. Rubira, A. B. Neto, P. Alessio, C. J. L. Constantino Surface-enhanced raman scattering for dopamine in Ag colloid: Adsorption mechanism and detection in the presence of interfering species, Appl. Surf. Sci., 522(2020) 146466.

[21] C. Papandreou, J. Li, L. Liang, M. Bulló, Y. Zheng, M. R. Canela, E. Yu, M. G. Ferré, C. Razquin, C. Clish, D. Corella, R. Estruch,

E. Ros, M. Fitó, F. Arós, L. S. Majem, N. Rosique, M. A. M. González, F. B. Hu, J. S. Salvadó, Metabolites related to purine catabolism and risk of type 2 diabetes incidence; modifying effects of the TCF7L2-rs7903146 polymorphism, Sci. Rep., 9(2019) 2892.

[22] O. A. Snytnikova, L. V. Yanshole, I. A. Iskakov, V. V. Yanshole, V. V. Chernykh, D. A. Stepakov, V. P. Novoselov, Y. P. Tsentalovich, Quantitative metabolomic analysis of the human cornea and aqueous humor, Metabolomics, 13(2017) 152.

[23] L. Liao, Y. Xing, X. Xiong, L. Gan, L. Hu, F. Zhao, Y. Tong, S. Deng, An electrochemical biosensor for hypoxanthine detection in vitreous humor: A potential tool for estimating the post-mortem interval in forensic cases, Microchem. J., 155(2020) 104760.

[24] D. Garg, M. Singh, N. Verma, Monika, Review on recent advances in fabrication of enzymatic and chemical sensors for hypoxanthine, Food Chem., 375(2022) 131839.

[25] M. E. Mendelsohn, D. H. Abramson, S. Senft, C. A. Servodidio, P. H. Gamache, Uric acid in the aqueous humor and tears of retinoblastoma patients, Journal of AAPOS, 2(1998) 369-371.

[26] B. K. Ghiam, L. Xu, J. L. Berry, Aqueous Humor Markers in Retinoblastoma, a Review, Transl. Vis. Sci. Technol., 8(2019) 13.

[27] S. Choi, S. W. Moon, S. H. Lee, W. Kim, S. Kim, S. K. Kim, J. H. Shin, Y. G. Park, K. H. Jin, T. G. kim, A recyclable CNC-milled microfluidic platform for colorimetric assays and label-free aged-related macular degeneration detection, Sens. Actuators B Chem., 290(2019) 484-492.

[28] W. Kim, S. H. Lee, S. H. Kim, J. C. Lee, S. W. Moon, J. S. Yu, S. Choi, Highly reproducible Au-decorated ZnO nanorod array on a graphite sensor for classification of

human aqueous humors, ACS Appl. Mater. Interfaces, 9(2017) 5891-5899.

[29] S. H Lee, S. Kim, J. Y. Yang, C. W. Mun, S. Lee, S. H. Kim, S. G. Park, Hydrogel-assisted 3D volumetric hotspot for sensitive detection by surface-enhanced raman spectroscopy, Int. J. Mol. Sci., 23(2022) 1004.

[30] I. B. Ansah, D. Aranda, H. S. Jung, S. G. Park, M. Kang, J. C. Otero, D. H. Kim, Dual synergistic modulation of photo-induced electron transfer processes between molecules and gold nanopillars for ultrasensitive plasmon-enhanced Raman scattering, J. Mater. Chem. C, 9(2021) 8842-8848.

[31] I. B. Ansah, T. An, J. Y. Yang, H. S. Jung, C. W. Mun, S. Jung, S. Lee, Y. Jang, D. H. Kim, M. Kim, S. G. Park, Electrochemical synthesis of 3D plasmonic-molecule nanocomposite materials for in situ label-free molecular detections, Adv. Mater. Interfaces, 8(2021) 2101201.

[32] S. Gunasekaran, G. Sankari, S. Ponnusamy, Vibrational spectral investigation on xanthine and its derivatives—theophylline, caffeine and theobromine, Spectrochim. Acta A Mol. Biomol. Spectrosc., 61(2005) 117-127.

[33] F. M. Miranda, A. Pedone, M. M. Miranda, Raman and computational study on the adsorption of xanthine on silver nanocolloids, ACS Omega, 3(2018) 13530-13537.

[34] M. Arivazhagan, S. Jeyavijayan, FTIR and FT-raman spectra, assignments, ab initio HF and DFT analysis of xanthine, Spectrochim. Acta A Mol. Biomol. Spectrosc., 79(2011) 161-168.

[35] J. Chowdhury, K. M. Mukherjee, T. N. Misra, A pH dependent surface-enhanced Raman scattering study of hypoxanthine, J. Raman Spectrosc., 31(2000) 427-431.

[36] W. Huang, J. Z. Jiang, L. Chen, B. Q. Zhang, S. F. Deng, J. J. Sun, W. K. Chen,

Density functional theory and surface enhanced Raman spectroscopy studies of tautomeric hypoxanthine and its adsorption behaviors in electrochemical processes, Electrochim. Acta, 164(2015) 132-138.

[37] S. H. Lee, W. C. Lee, E. H. Koh, I. B. Ansah, J. Y. Yang, C. W. Mun, S. Lee, D. H. Kim, H. S. Jung, S. G. Park, Organometallic hotspot engineering for ultrasensitive EC-SERS detection of pathogenic bacteria-derived DNAs, Biosens. Bioelectron., 210(2022) 114325.

[38] I. B. Ansah, S. H. Lee, C. W. Mun, D. H. Kim, S. G. Park, Interior hotspot engineering in Ag-Au bimetallic nanocomposites by in situ galvanic replacement reaction for rapid and sensitive surface-enhanced raman spectroscopy detection, Int. J. Mol. Sci., 23(2022) 11741.

[39] H. Tian, N. Zhang, J. Zhang, L, Tong, Exploring quantification in a mixture using graphene-based surface-enhanced Raman spectroscopy, Appl. Mater. Today, 15(2019) 288-293.